*metals*

MDPI

*Article*

# Research on the Microstructure and Mechanical Properties of Repaired 7N01 Aluminum Alloy by Laser-Directed Energy Deposition with Sc Modified Al-Zn-Mg

**Jibing Chen [1], Shanji Yu [1], Junsheng Yang [1,*], Rong Xu [2], Ruidi Li [2], Shisen Huang [1], Hongbin Zhu [3] and Xinyan Liu [2]**

[1] School of Mechanical Engineering, Wuhan Polytechnic University, Wuhan 420023, China
[2] State Key Laboratory of Powder Metallurgy, Central South University, Changsha 410083, China
[3] CRRC Industrial Research Institute, Beijing 100053, China
* Correspondence: yangjunsheng2008@163.com

**Abstract:** Aluminum alloy is an important material used in railway train structures. It is of great significance to repair aluminum alloy through directional energy deposition to reduce cost and improve the performance of the aluminum alloy. In this study, 7N01 aluminum alloy was repaired by means of laser-directed energy deposition (DED) with the powder of Sc-modified Al-Zn-Mg aluminum alloy as raw material. The microstructure and mechanical properties of the repaired specimens were studied through the metallographic microscope, scanning electron microscope, electron backscatter diffraction, universal tensile test, and Vickers hardness test in combination. The results show that the bonding interface of the repaired aluminum alloy is satisfactory, and the porosity is 2.8%. The grains in the repaired area are the columnar crystals growing vertically along the boundary of the melt pool with an obvious temperature gradient. Fine equiaxed crystals are distributed along the boundary of the melt pool, and $Al_3(Sc,Zr)$ particles play a role in grain refinement. The average grain size of the fine grain area in the repair zone next to the fusion zone is 9.1 μm, and the average grain size of the coarse grain area is 20 μm. The average tensile strength in the area of repair approaches 349 MPa, which is 91% that of the base material, and the elongation rate is 10.9%, which is 53.2% that of the base material. The hardness ranges between 122 HV and 131 HV, which is comparable to the base material. However, there is a significant decrease in the tensile strength and hardness of the base material (heat-affected zone).

**Keywords:** Sc modification; DED; microstructure; mechanical property; heat-affected zone

check for updates

**Citation:** Chen, J.; Yu, S.; Yang, J.; Xu, R.; Li, R.; Huang, S.; Zhu, H.; Liu, X. Research on the Microstructure and Mechanical Properties of Repaired 7N01 Aluminum Alloy by Laser-Directed Energy Deposition with Sc Modified Al-Zn-Mg. *Metals* **2023**, *13*, 829. https://doi.org/10.3390/met13050829

Academic Editors: Joan-Josep Suñol and Leszek Adam Dobrzański

Received: 12 March 2023
Revised: 12 April 2023
Accepted: 18 April 2023
Published: 23 April 2023

**Copyright:** © 2023 by the authors. Licensee MDPI, Basel, Switzerland. This article is an open access article distributed under the terms and conditions of the Creative Commons Attribution (CC BY) license (https://creativecommons.org/licenses/by/4.0/).

## 1. Introduction

With various advantages such as high strength, good plasticity, and high performance in corrosion resistance, aluminum alloy can effectively reduce the self-weight of components and maintain a certain level of strength and toughness. Therefore, it plays an important role in promoting the application of large-sized complex aluminum alloys in trains. When the train is operational in a harsh environment for long, the components made of aluminum alloy tend to be damaged (such as wearing, stress corrosion, and fatigue crack), which can lead to failure, thus posing safety risks to the passengers onboard [1]. Therefore, the prompt repair of damaged parts can not only reduce operational costs but also ensure the safety of passengers. With a laser beam as the source of energy, a closed-loop control system is applied to produce the metallic components that can be used to control dimensional accuracy, physical integrity, and full density [2]. Due to the high thermal conductivity and surface reflectivity of aluminum, heat tends to accumulate in the course of processing, thus resulting in cracks and holes. Therefore, high laser power and an appropriate scanning speed are required to melt aluminum alloy powder. With the increase of laser energy, the alloying elements with a low boiling point, such as zinc and magnesium,

are selectively evaporated, which may lead to a decrease in the porosity and mechanical properties of the deposited samples [3].

Due to the high coefficient of thermal expansion, high-temperature ranges from liquids to dissolved phase line, and significant shrinkage after solidification, Al-Zn-Mg alloy is prone to cracking when DED solidifies rapidly. The extensive thermal cracking in Al-Zn-Mg alloys produced with laser additives causes deterioration in their properties, even to the extent that they are inferior to conventionally processed alloys. In general, the composition of aluminum alloy determines the development of hot cracks, so optimizing the composition of the alloy can be effective in reducing or preventing the generation of hot cracks [4]. Anika Langebeck et al. used DED to print EN AW-7075 alloy by increasing laser power to extend degassing, which not only improves hardness and strength but also reduces porosity, with the tensile strength reaching up to (222 $\pm$ 17) MPa [5]. M.J. Benoit printed Al 7075 alloy by adjusting various parameters of laser processing, such as laser power, scanning speed, and mass flow rate. With the extensive solidification-induced cracks eliminated, the porosity falls below 1% [6]. Wang Xiaoyan et al. repaired 7050 aluminum alloy with $AiSi_{12}$ and effectively inhibited the development of pores and cracks by optimizing process parameters and changing the state of the powder [7].

The DED process is characterized by rapid solidification, and solidification-induced cracking is a problem discovered in 7xxx alloy DED. It has been indicated that introducing a small amount of Sc to 7 series aluminum alloy can provide the nucleation sites required to promote the formation of equiaxed grain $Al_3$(Sc,Zr), which makes it more resistant to cracking than columnar grain when solidifying, thus improving its mechanical properties [4,8]. Pan Wei et al. used laser selective melting (SLM) to print Al-6.2Zn-2Mg-xSc-xZr alloy and studied the microstructure characteristics of Al-6.2Zn-2Mg-xSc-xZr alloy with different Sc and Zr contents, as well as the influence mechanism of Sc and Zr on cracking. The research results indicate that with the increase of Sc and Zr content, the crack trend and grain size in the printed samples decrease. When the Sc and Zr contents reach 0.6% and 0.36%, respectively, cracks no longer appear in the printed sample [9]. Bi Jiang et al. obtained SLM samples under different process parameters by mixing low microalloy content (0.4 wt% Sc and 0.25 wt% Zr) with Al 7075 powder. According to the results, a higher laser energy density is conducive to reducing microcracks and refining grains, which significantly improves compressive strength [10].

It has been revealed in plenty of studies that the heat-treatable aluminum alloy softens in the heat-affected zone after welding, which is mainly attributed to the "over-aging" of the zone at high welding temperatures. That is to say, the second phase cograted with the aluminum matrix is precipitated, agglomerates, and grows, thus reducing the strengthening effect [11]. Li Nianjun et al. took 7075-T6 aluminum alloy as a plate for friction stir processing, with the research results showing that the mechanical properties (tensile strength and elongation) deteriorated significantly after friction stir processing [12]. The temperature of 7xxx aluminum alloy in the DED process is higher, and a similar situation occurs. At present, there has been a lot of research conducted on the laser welding of 7 series aluminum alloys both at home and abroad [13]. However, there are still few reports on the laser repair of 7 series aluminum alloy, especially DED technology. In the present study, Sc-modified Al-Zn-Mg alloy powder is used to explore the approach to laser additive repair of 7N01 aluminum alloy for an in-depth analysis of the microstructure and mechanical properties of the repaired samples. This is purposed to provide a theoretical reference for the laser repair technology applicable to 7 series aluminum alloy.

## 2. Materials and Methods

### *2.1. Experimental Methods and Materials*

The base material used in this study is 7N01 (annealed) aluminum alloy. In the base plate sized 150 mm $\times$ 100 mm $\times$ 11 mm, a groove is opened to simulate the damage. Then, the aluminum alloy base plate to be repaired is slotted, whose cross-section is shown in Figure 1. The surface of the groove is 9 mm in length, 4 mm in height, and 1 mm in length

at the bottom. Table 1 lists the composition and tensile properties of the matrix materials at room temperature. The raw material used for repair is an aerosolized gas powder of Sc-modified Al-Zn-Mg alloy, whose composition is tested by inductively coupled plasma emission spectrometer, as shown in Table 2. The average particle size ranges from 92 to 143 μm.

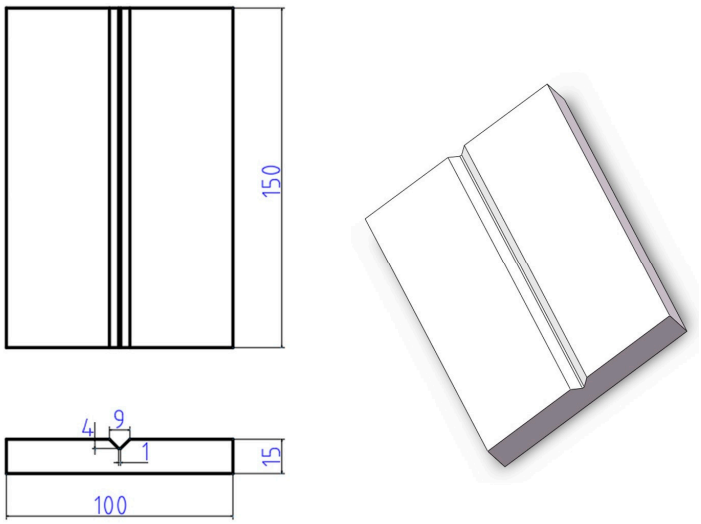



**Figure 1.** 7N01 substrate prefabricated V size diagram (Unit: mm).

**Table 1.** Composition and mechanical properties of matrix material (7N01 aluminum alloy).

| Alloy | Mg | Mn | Fe | Cr | Si | Zn | Cu | Ti | Al | Tensile Strength (MPa) | Yield Strength (MPa) | Elongation (%) |
|---|---|---|---|---|---|---|---|---|---|---|---|---|
| 7N01 | 1.50 | 0.4 | 0.35 | 0.30 | 0.30 | 4.50 | 0.20 | 0.20 | Bal. | 383 | 330 | 20 |

**Table 2.** Composition of matrix material (mass fraction, %).

| Zn | Mg | Sc | Zr | Si | Mn | Cu | Cr | Ti | V | Al |
|---|---|---|---|---|---|---|---|---|---|---|
| 4.80 | 4.06 | 0.70 | 0.12 | 0.40 | 0.48 | 0.21 | 0.30 | 0.09 | 0.09 | Bal. |

Produced by Nanjing Zhongke Yuchen Laser Technology Company, LDM8060 laser-oriented energy deposition equipment (Nanjing Zhongke Yuchen Laser Technology Co., Ltd., Nanjing, China) was used to perform the experiment. It consisted of a powder feeder, a protective gas system, a programming computer, a laser system, and a CNC-forming cabin body (sealed cabin, five-axis forming table, laser powder coaxial nozzle). The spot diameter was 2.5–3.0 mm. The maximum laser power was 2000 W, and the maximum scanning speed was 800 mm/min. In the process of repair, argon was taken as the protective gas, and the repair started when the oxygen volume fraction in the chamber fell below 300 PPM. In order to ensure a satisfactory interface of repair, the size of the inverted mold of the groove was set to 1.1 times that of the matrix groove. The parameters of laser-oriented energy deposition repair are as follows: a scanning speed of 600 mm/min, a laser power of 1600 W, a scanning interval of 1.2 mm, a layer thickness of 0.5 mm, a powder feed speed of 0.8 r/min, and an argon flow rate of 4 L/min. Prior to the experiment, the surface of the groove was polished using sandpaper to remove the oxidation layer. Moreover, Sc-modified Al-Zn-Mg aluminum alloy powder was placed in a vacuum drying oven at 120 °C for 2 h so as to remove moisture from the powder for a better combination with the base material.

### *2.2. Sample Preparation*

After the repair of the 7N01 aluminum alloy sample was completed, the electric discharge wire cutting machine was employed to cut and sample the groove in the horizontal and vertical directions for examination of the mechanical properties and microstructure of the interface between the base material and the repair area. Hot insertion was performed using metallographic inlaying powder and cut-off samples on the metallographic sample inlaying machine. After cooling, the sandpaper (320#, 800#, 2000#, 3000#, 5000#) was taken out for sanding on the metallographic sample polishing machine (BMP-2DE). Then, silica sol was added into the metallographic automatic grinding machine for polishing until there was no obvious scratch. After wiping, the sample was etched with Kohler reagent (1.0 mL HF + 1.5 mL HCL + 2.5 mL $HNO_3$) for 15 s, rinsed with water, and dried with a hair dryer. The microstructure and composition of a specimen were observed and analyzed by means of Optical Microscopy (OM) (Light Mirror Technology Co., Ltd., Suzhou, China), Quanta200 (FEI) type Scanning Electron Microscopy (Hangzhou Ritsch Technology Co., Ltd., Hangzhou, China), and Electron Backs Scattered Diffraction (Beijing Jingyi Automation Equipment Technology Co., Ltd., Beijing, China).

In the experiment, the sample was cut by the electric spark wire cutting machine, and 3 tensile samples were cut at a point 2 mm away from the edge of repaired part of the aluminum alloy. Figure 2 shows the method of sampling and the size of the tensile samples. The electronic universal tensile testing machine was used to conduct tests on the tensile properties of the repaired aluminum alloy samples, including tensile strength, yield strength, and elongation. A MICROMET 5104 microhardness tester (Hangzhou Duuandi Testing Equipment Co., Ltd., Hangzhou, China) was employed to measure the hardness from the area of repair near the fusion line to the matrix every 0.4 mm for 15 s.

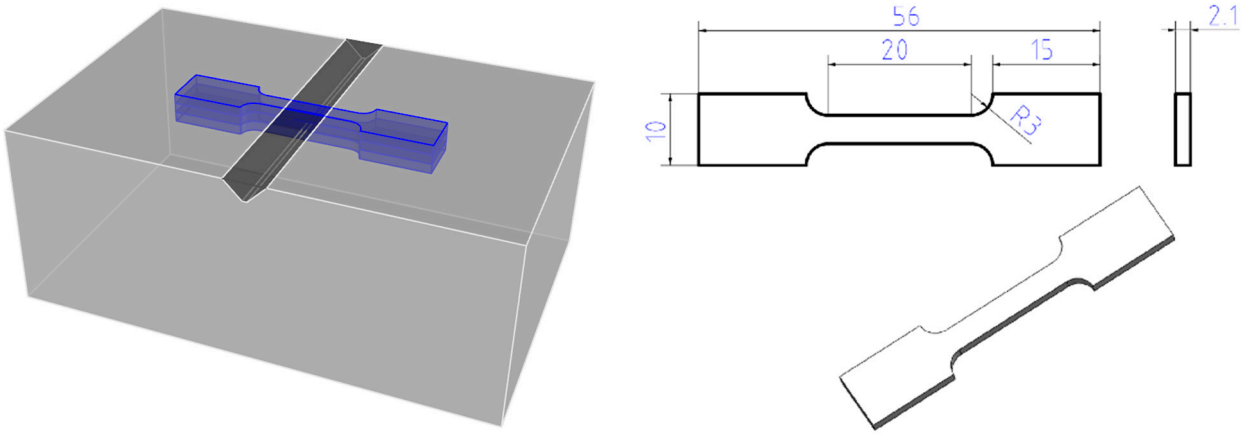



**Figure 2.** Sampling method and size of drawing sample of 7N01 aluminum alloy repaired by laser additive at room temperature (Unit: mm).

## 3. Results

### *3.1. Microstructure of Deposition Sample of Sc Modified Al-Zn-Mg Alloy Powder*

Figure 3 shows the microstructure of Sc-modified Al-Zn-Mg prealloy powder deposition samples obtained by DED. As can be seen from Figure 3a,b, there are basically no cracks in the alloy except a few holes in the molten pool. This is because of the application of DED as the quick-cooling and hot-quenching technology and the high cooling rate of the molten pool. The porosity defects result mainly from the rapid penetration of a small amount of gas (Zn and Mg) into the sedimentary layer without time allowed to overflow [6]. It can be seen from the enlarged area of the metallographic diagram that the grains are relatively fine and uniform, which is due to the process of crystal nucleation and growth under a higher temperature gradient. The higher cooling rate limits the growth of the crystal lattice and reduces the size of the grains. In addition, $MgZn_2$ precipitates exist in the

grain boundary, which can play the role of precipitation strengthening [4], and $Al_3(Sc,Zr)$ plays the role of grain refinement.

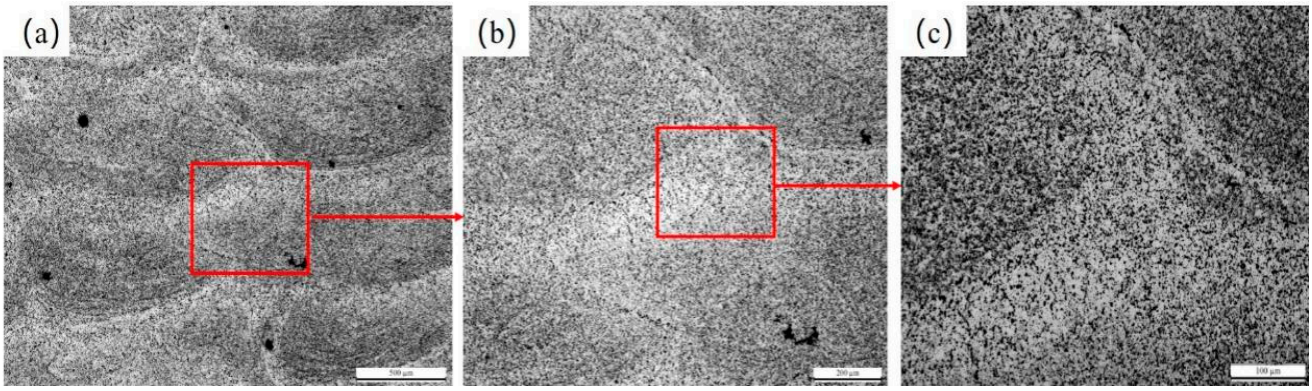



**Figure 3.** Sc modified Al-Zn-Mg pre-alloy powder deposition sample OM: (**a**) ×500; (**b**) corresponding to the framed area in (**a**); (**c**) corresponding to the framed area in (**b**).

Table 3 shows the mechanical properties of deposition samples of Sc-modified Al-Zn-Mg prealloy powder as formed by DED, and Figure 4 shows the engineering stress–strain curve. It can be seen from the table that the average tensile strength of the alloy is 311.6 MPa, the average elongation rate is 15.6%, and the overall mechanical properties are excellent.

**Table 3.** Mechanical properties of Sc-modified Al-Zn-Mg prealloy powder deposition samples.

| Number | Laser Power, P (W) | Scanning Speed, V (mm/min) | Yield Strength (MPa) | Tensile Strength (MPa) | Elongation (%) |
|---|---|---|---|---|---|
| 5-1 | 1600 | 600 | 183 | 325 | 18.2 |
| 5-2 | 1600 | 600 | 180 | 310 | 15 |
| 5-3 | 1600 | 600 | 180 | 300 | 13.8 |

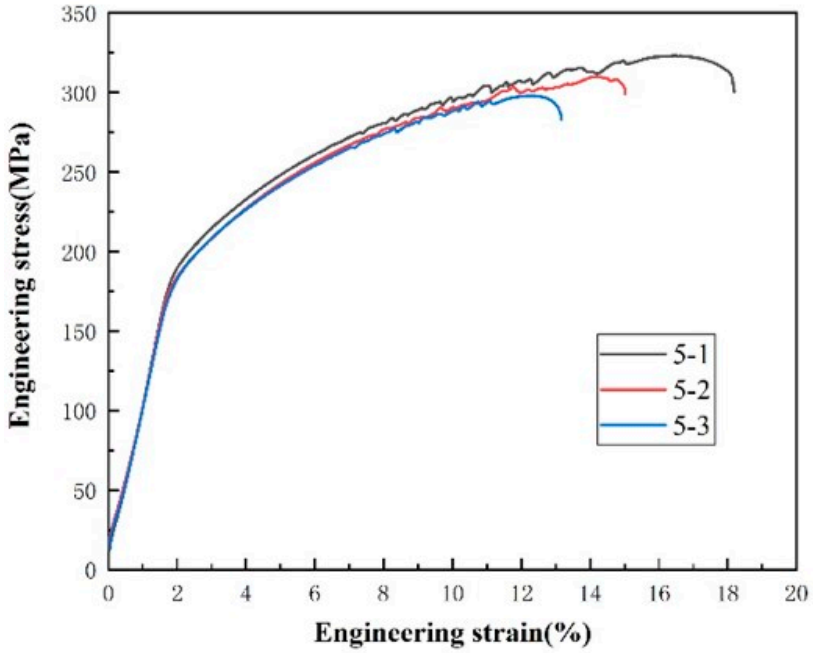



**Figure 4.** Engineering stress–strain curves of Sc-modified Al-Zn-Mg prealloy powder (P = 1600 W, V = 600 mm/min) deposited by DED.

### *3.2. Microstructure Analysis of Repair Parts*

Figure 5 shows the metallographic assemblages of 7N01-T5 repaired by Sc-modified Al-Zn-Mg prealloy powder at different ratios in different regions. According to the panoramic view of the metallographic structure, the fusion interface is well bonded with no cracks observed. The Image Pro-Plus software was used to calculate the porosity of the selected triangle area in the restoration area, and the porosity was 2.8%. As shown in Figure 5a, the fishscale-like layered structure similar can be observed in the area of repair, which is mainly caused by the partial remelting of the sedimentary layer tissue and the coarsing by heat. After the corrosion by Kohler's reagent, the phenomenon of dark and dark phases is more obvious under the optical microscope [14]. Careful observation showed that there were more holes in the upper part of the restoration area, and they were larger. The holes in the lower part of the restoration area were few and small. This is because the temperature of the substrate contact part decreases quickly, and the light elements such as Zn and Mg are allowed no time to evaporate. Since the temperature decreases slowly in the upper part of the area of repair, the evaporation of Zn and Mg elements is more serious, resulting in more holes [1,15].

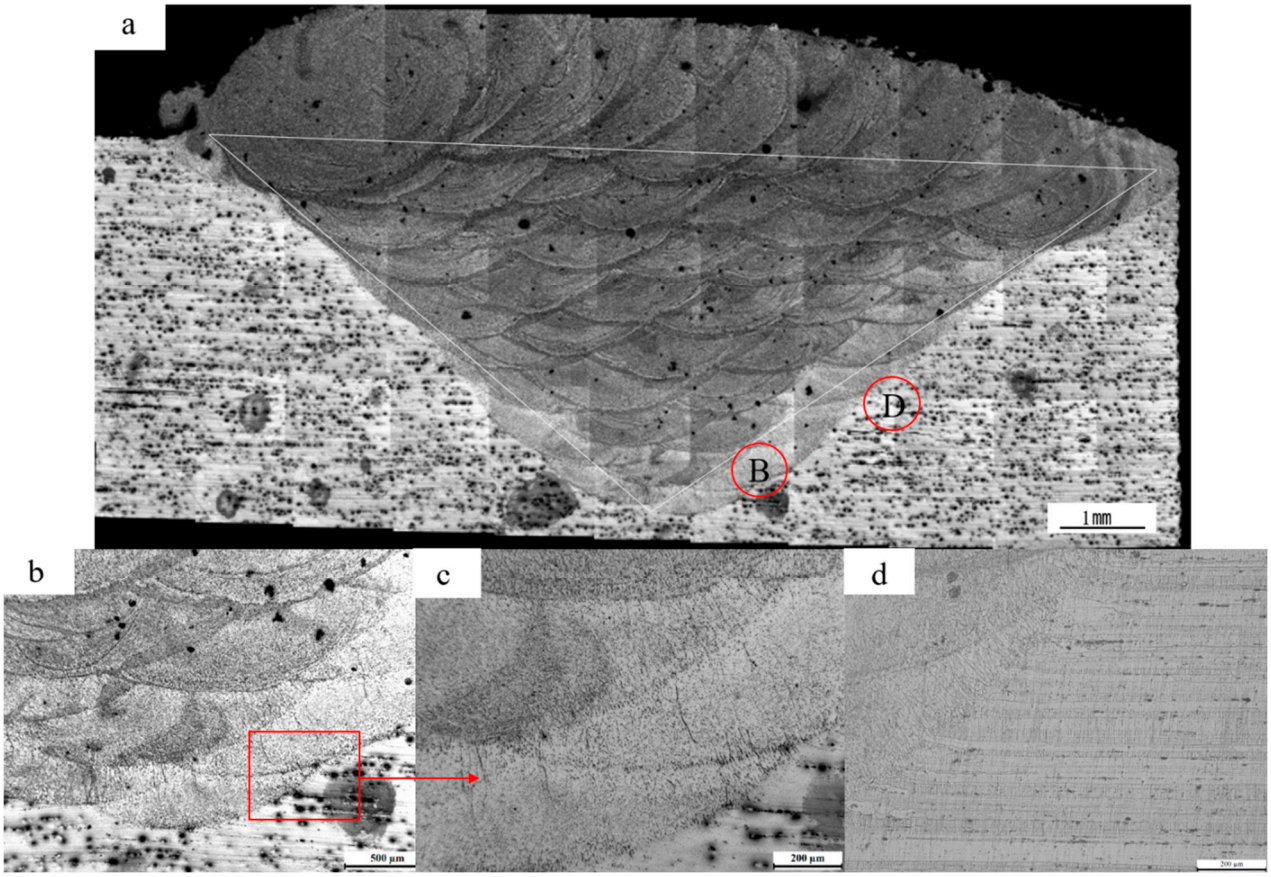



**Figure 5.** Panoramic and local enlarged image of OM of metallographic section in the restoration area, (**c**) corresponding to the framed of (**b**), (**b**,**d**) corresponding to (B) and (D) in (**a**), respectively.

The grains distributed at the boundary of repair are fine equiaxed grains, and the appearance of fine equiaxed grains at this position is not only related to the large temperature gradient but also to the accumulation of $Al_3(Sc,Zr)$ particles, which can play a role in grain refinement [9,16]. From the areas indicated in Figure 5b,c, it can be seen that the grain in the fusion zone is columnar and grows vertically along the boundary of the molten pool. This phenomenon is more obvious at the bottom of the repaired groove because the bottom part of the groove was deposited first. At this time, the temperature of the base metal is low,

and the direction of the temperature gradient is obvious. From Figure 5d, it can be seen that the orientally-growing columnar crystals at the top of each sedimentary layer transform into equiaxed crystals. This is because the top of the sedimentary layer not only dissipates heat between layers but also dissipates heat through the substrate [17]. The grains in the base material (matrix) region are distributed in coarse bands.

The DED process is characterized by a high-temperature gradient and fast cooling rate, which involves a rapid solidification process. The sediments release heat in three main ways, first through the conduction of adjacent laminar currents, then into the basement, and finally into the nearby atmosphere through convection and radiation. In this process, heat flows mainly through the adjacent sedimentary layers and the basement, and the influence caused through the atmosphere is quite limited [2,17]. Figure 6 shows the morphology of repaired parts of the aluminum alloy as observed under a scanning electron microscope. These parts are divided into a repair zone, fusion zone (transition zone), heat-affected zone (solid solution zone, over-aging zone), and matrix. According to Figure 6b,c, there are white spot-shaped and square-shaped $Al_3(Sc,Zr)$ particles distributed in the restoration area, which plays a role in the refinement of grains.

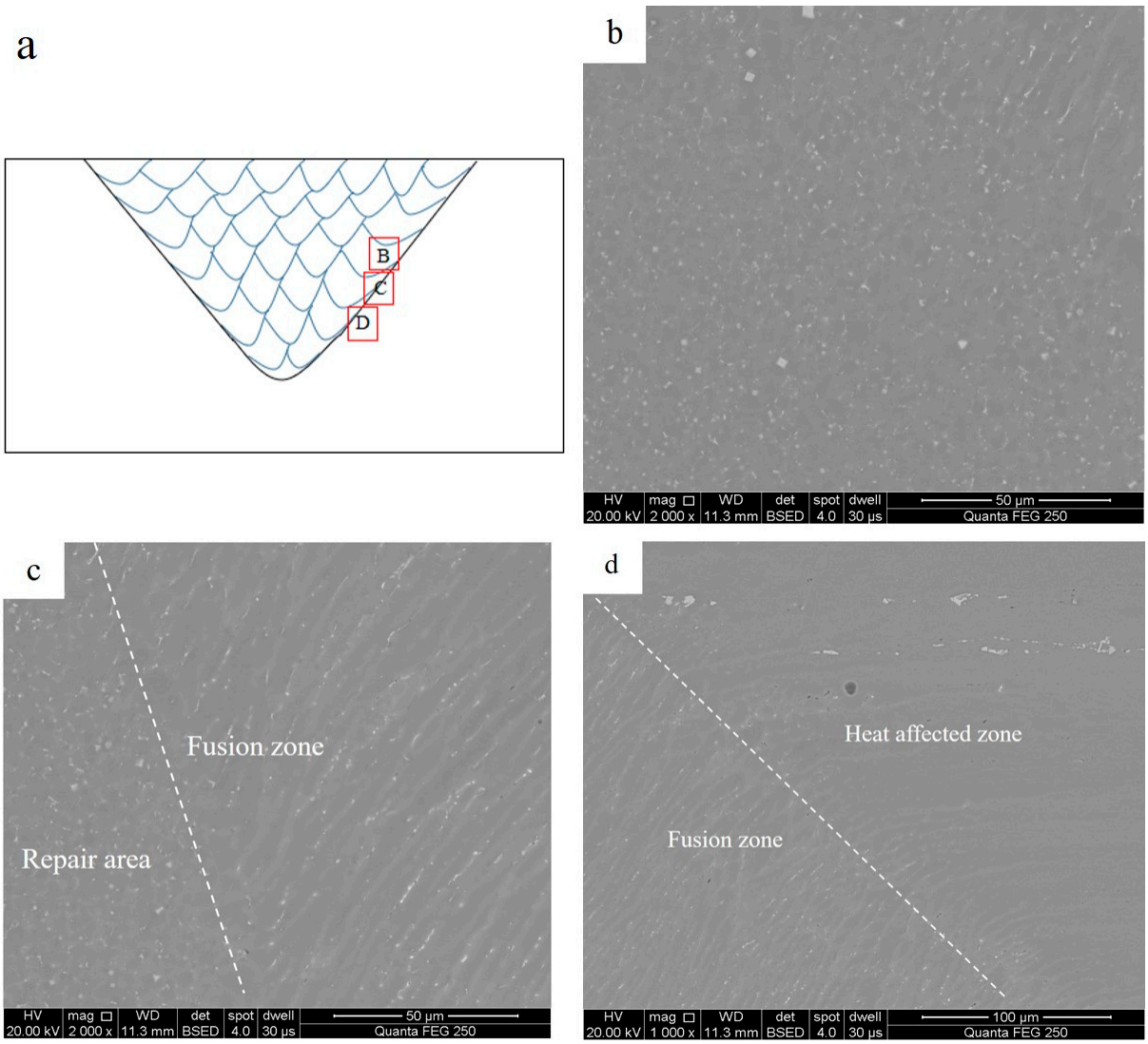



**Figure 6.** SEM diagram of various tissues of repair sample, (**b**–**d**) corresponding to the positions of (B–D) in (**a**), respectively.

In order to study the composition in the restoration area, an EDS scanning analysis was conducted in the restoration area, as shown in Figure 7. According to this figure, element segregation is observable. Mg, Si, and Sc are enriched in the restoration area, with a small number of elements Zr, Zn, and Mn observed. It is demonstrated that the introduction of the Sc element into aluminum alloy is effective in promoting grain refinement and inhibiting recrystallization. Moreover, the strengthening effect of solid solution is enhanced with the increase of Si content in the matrix. Due to the rapid cooling in the DED process, non-equilibrium solidification is easy to occur, leading to the interdendrite segregation of solute atoms. The main strengthening elements, such as Mg and Zn, are still solid solutions in the a-Al matrix, and $MgZn_2$ intermetallic phases are easy to form in grain boundaries and grains [18].

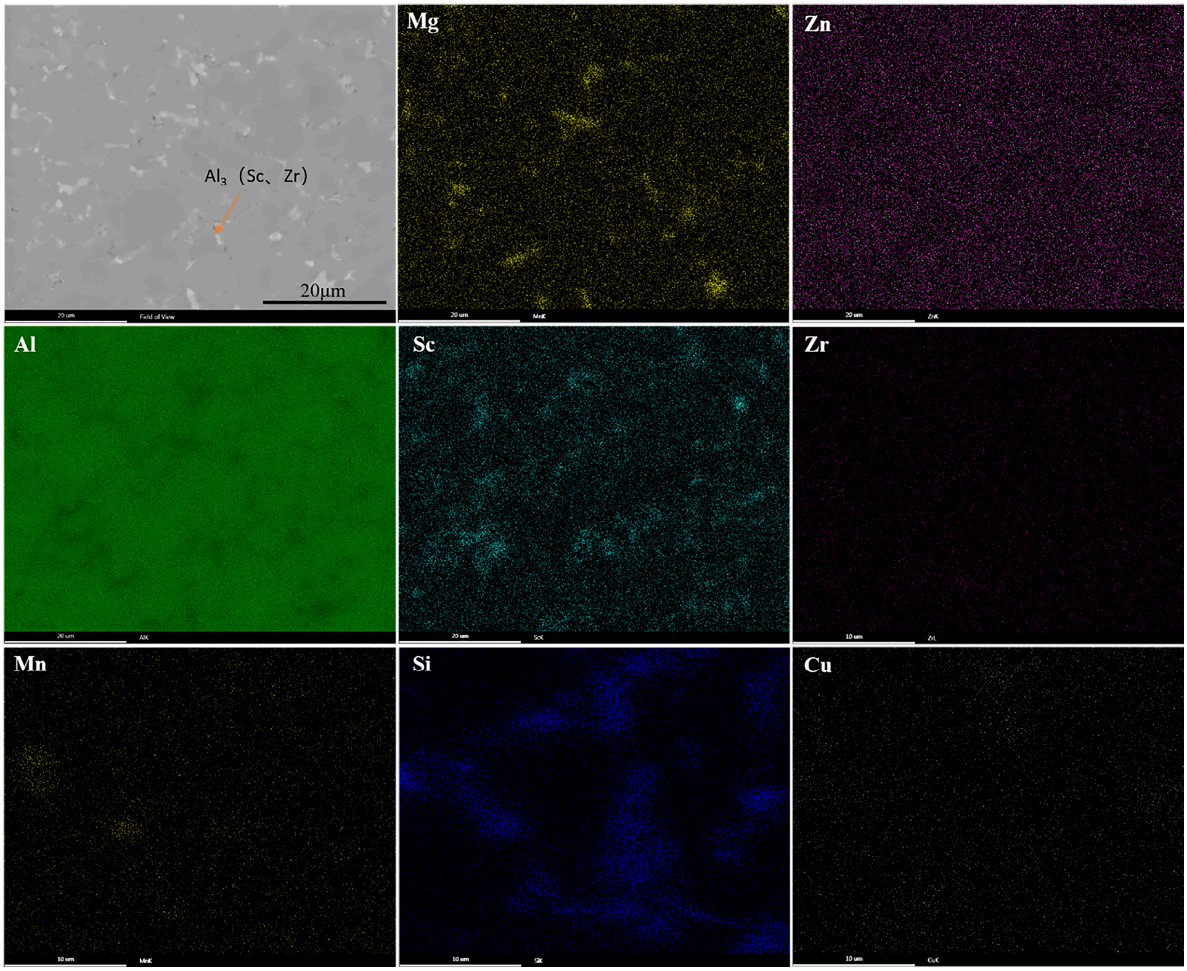



**Figure 7.** SEM image of distribution of Al, Zn, Mg, Sc, Zr, Mn, Si, and Cu elements in the restoration area.

Figure 8 shows a scan of EBSD (Electron Backs Scattered Diffraction) and the distribution of its grain size at the boundary of fusion in a repaired specimen as prepared by electrolytic polishing. From Figure 8c, it can be clearly seen that the grain size from the repaired zone to the base material first increases, then decreases, and finally increases again. The average grain size in the coarse-grained zone and fine zone of the molten pool reaches 20 μm and 9.1 μm, respectively. As shown in Figure 8b, there are fine columnar crystals in the scanning channel region (fusion zone) of the bottom layer of equiaxed crystals with fine distribution in the optimum restoration area, and the upper columnar crystals are thicker. This is because the heat dissipation rate is faster in the bottom layer during the process of laser repair, and the liquid molten pool comes into contact with the base material, which

makes it easy to generate columnar crystals. The direction of columnar crystals' growth at this position is perpendicular to the fusion line. The microstructure of the base metal is comprised of coarse columnar crystals, which to some extent is attributed to the growth of grains in the heat-affected zone during repair [19,20].

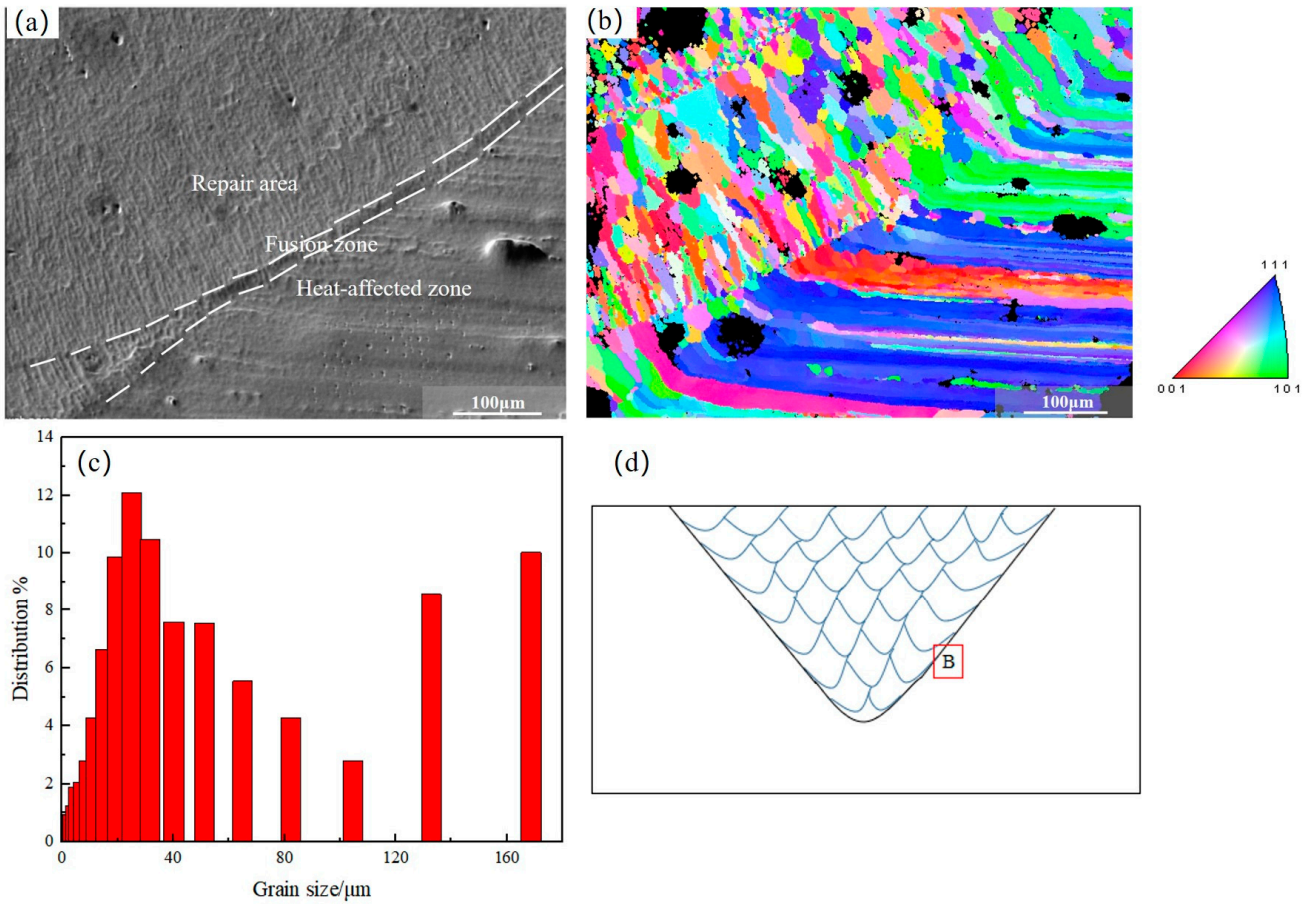



**Figure 8.** EBSD image and grain size of the transition region of the repaired sample: (**a**) EBSD; (**b**) Microstructure of fine columnar crystals; (**c**) Distribution of grain size; (**d**) Schematic diagram of fusion boundary.

### *3.3. Mechanical Properties and Hardness Analysis of Repair Parts*

According to the engineering stress–strain curve corresponding to Figure 9 and the mechanical properties of 7N01 repaired by Sc-modified Al-Zn-Mg in Table 4, the average tensile strength of 7N01 base metal (matrix before the repair) is 384 MPa, and the elongation rate is 20.5%. According to the section diagram of the repair zone in Figure 9, the tensile samples containing the repair zone (molten pool) were divided from top to bottom into the repair zone accounting for 71% and 29%. The tensile strength of the tensile samples with a large proportion of repair zone was significantly higher than that of those with a small proportion of repair zone. The average tensile strength of the tensile sample in the area of repair is 349 MPa, reaching 91% of that of the base material (the matrix before the repair), and the elongation rate is 10.9%, reaching 53.2% of that of the base material. The tensile properties of the matrix (heat-affected zone) under the repair zone decreased significantly, the tensile strength was only 269 MPa, and the elongation rate was 16.2%. This is because, in the repair process, if the repair sample was at too high a temperature for too long a time, the saturated solid solution would precipitate the equilibrium phase η ($MgZn_2$), thus forming a correlation with the matrix. When a large number of η phases precipitate, the second phase is coarsened by heat and the alloy significantly softens [21–23], thus reducing both tensile strength and hardness.

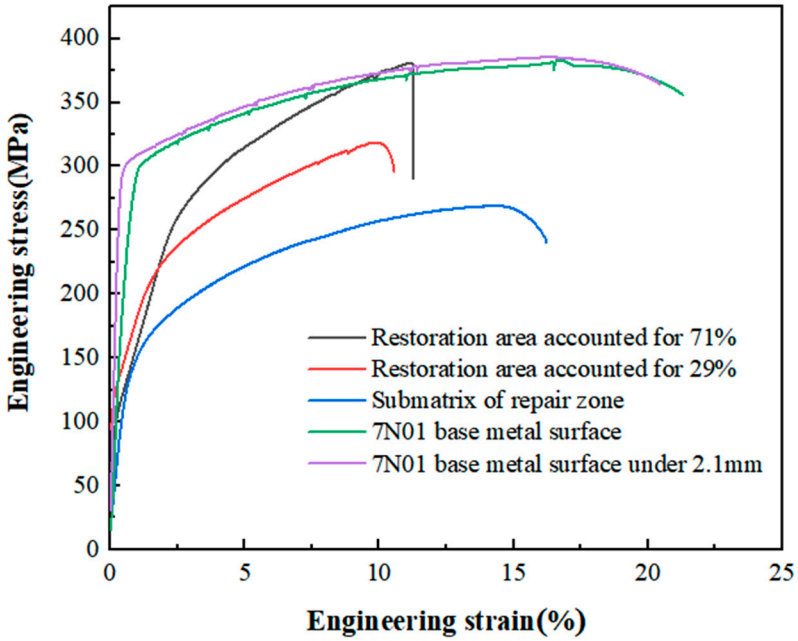



**Figure 9.** Engineering stress–strain curves of aluminum alloy repair parts and base metal.

**Table 4.** Mechanical properties of base metal and aluminum alloy repair parts.

| Sample Number | Yield Strength (MPa) | Tensile Strength (MPa) | Elongation (%) |
|---|---|---|---|
| Restoration area accounted for 71% | 250 | 381 | 11.3 |
| Restoration area accounted for 29% | 162 | 318 | 10.5 |
| Submatrix of repair zone | 124 | 269 | 16.2 |
| 7N01 base metal surface | 330 | 383 | 21 |
| 7N01 base metal surface under 2.1 mm | 335 | 385 | 20 |

In the process of the tensile test, the fracture trace of the tensile sample, including the repair zone, is found on the matrix, as shown in Figure 10. This is because the mechanical properties of the repair zone are better than that of the base material. Consequently, the matrix part is weak, which causes the sign of fracture to emerge on the matrix. The tensile properties of the repaired specimens are closely related to the structure of each region, reflecting the properties of each region. Figure 11a shows the SEM of fracture 1 of tensile specimen in the area of repair, and Figure 11b–d show the SEM of each position under different parameters in Figure 11a. Despite the flat areas in Figure 11c,d as a result of grinding in the process of sample preparation, there remain a large number of dimples observed from the regional drawings, especially in Figure 11b. Thus, it was judged as a ductile fracture.

Figure 12 shows the side hardness of the repaired sample made of aluminum alloy, with the average hardness of the base metal reaching 131 HV. The hardness in the restoration area exceeds 120 HV, and the highest hardness is shown by 7N01 base metal. There is a significant decrease in the interface hardness of the repair zone, which is because the solid solution zone (heat-affected zone) is formed after the powder material melts and mixes with the matrix to resolidify. In this area, its composition and microstructure are not uniform. Additionally, the thermal cycle temperature is fairly high, which results in the partial or complete melting of the demelting phase of aluminum alloy into the matrix [13,16], whose hardness varies between 90 HV and 126 HV. The over-aging zone (heat-affected zone) underwent a low peak heat drive, which converts the metastable phase into a stable phase, thus eliminating the semi-coherent relationship with the matrix. Consequently, the hardness is reduced to the minimum, ranging between 83 and 90 HV. The hardness from the aging zone to the matrix fluctuates around 83 HV. Due to the large temperature gradient

in the DED process, the substrate softens, and the level of hardness decreases, which is consistent with the mechanical properties tested before.

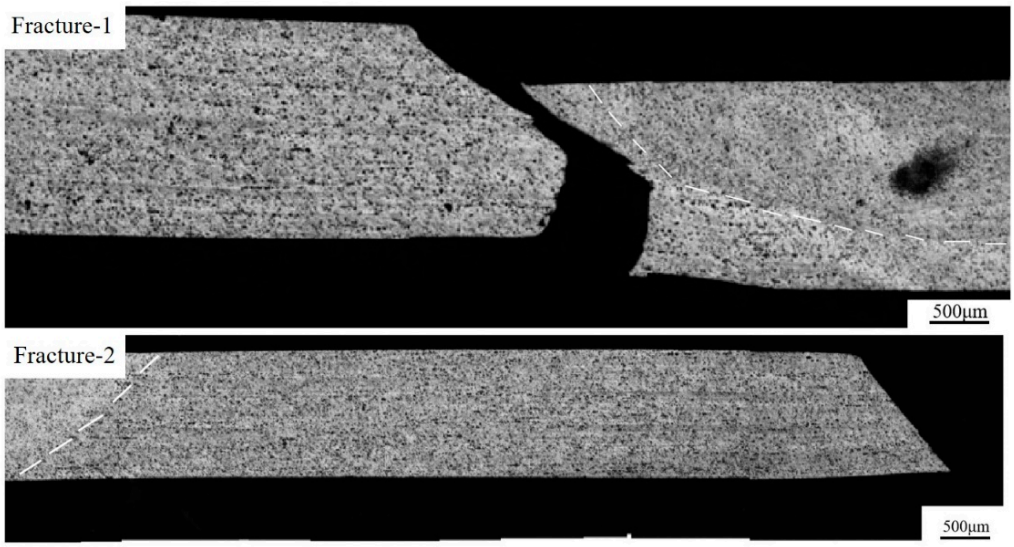



**Figure 10.** OM diagram of fracture position of tensile specimen in repair area.

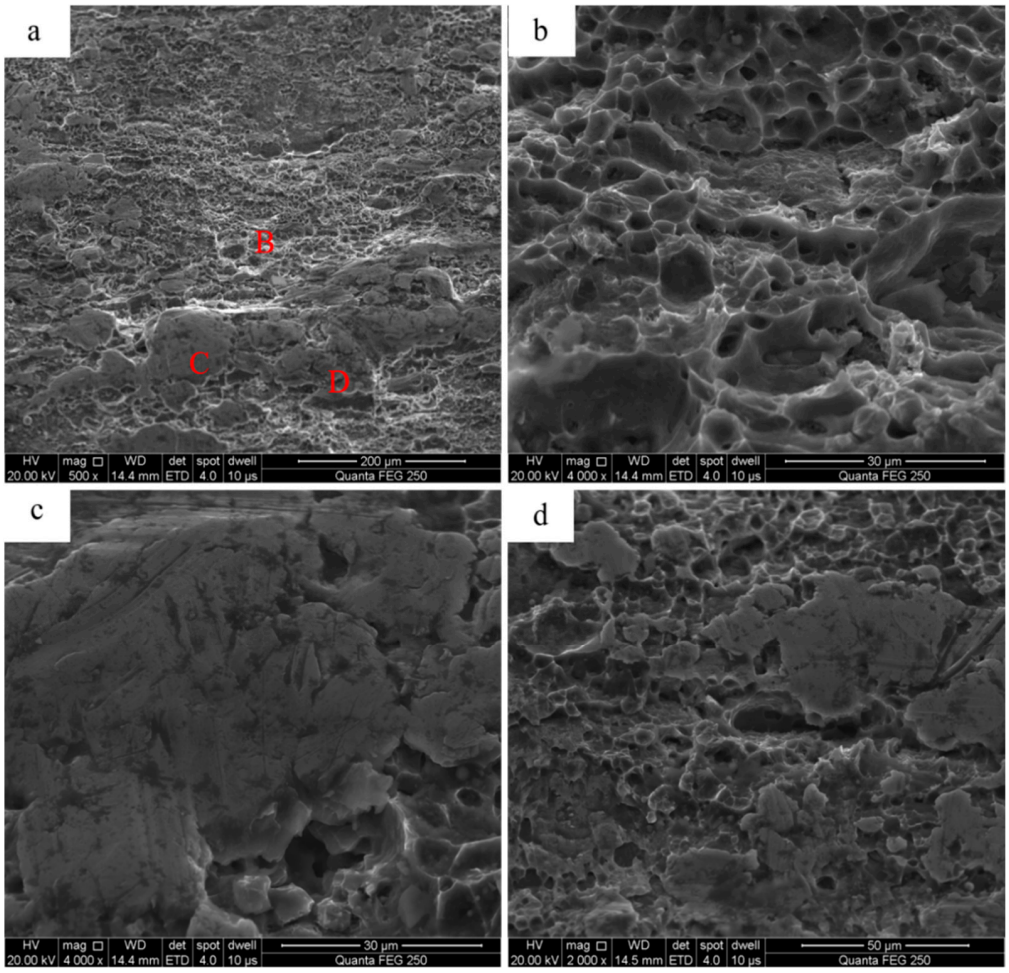



**Figure 11.** SEM image of tensile fracture in the repair area at room temperature, (**b**–**d**) corresponding to (B–D) in (**a**), respectively.

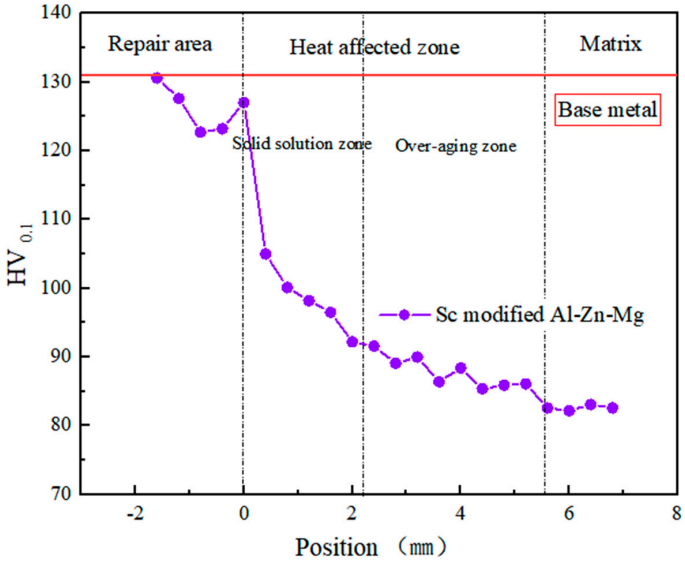



**Figure 12.** Hardness distribution on the side of the repaired sample.

In order to address the softening of the substrate, there are two methods proposed. One is to reduce the speed between the printing layers in the printing process to avoid substrate heat dissipation. The other is heat treatment, with a method of solution plus aging adopted for the repaired parts of DED after normal repair. For solid solutions, increasing the solution temperature can improve the solubility of coarse second-phase particles. For aging, high alloy content increases the sensitivity of alloy temperature. Solid solution + aging treatment can be carried out to reduce the non-melted coarse second phase, thus improving the mechanical properties of the alloy [24].

## 4. Summary

(1) Given the appropriate technological parameters, 7N01 aluminum alloy was repaired with Sc-modified Al-Zn-Mg aluminum alloy powder with a porosity of 2.8% but no cracks. Despite a few pores, the overall density was satisfactory.

(2) The repair zone can be divided into the area of repair, fusion zone, heat-affected zone, and matrix. The range of the heat-affected zone was stable after 5.8 mm. There were white spot-shaped and square $Al_3(Sc,Zr)$ particles found in the restoration zone, which played a role in refining the grain.

(3) The average tensile strength of the repaired sample was 349 MPa, reaching 91% that of the base material, and the elongation rate was 10.9%, reaching 53.2% that of the base material. Furthermore, the trace of fracture emerged on the base material. There was a sharp decline in tensile strength and hardness from the heat-affected zone to the matrix, which is attributed to the large temperature gradient in the DED process, thus leading to the softening of the substrate. As for the softening of heat affected zone of the substrate, its mechanical properties can be improved through heat treatment.

**Author Contributions:** Conceptualization, J.C., S.Y., R.X., R.L. and H.Z.; data curation, S.Y., J.C., R.X. and H.Z.; methodology, S.Y., R.X., J.C., R.L., X.L. and H.Z.; software, S.Y., S.H. and R.X.; validation, S.Y., S.H., R.L. and R.X.; writing—original draft preparation, S.Y.; writing—review and editing, J.C., S.Y., J.Y. and R.X.; project administration, S.Y., R.X. and R.L. All authors have read and agreed to the published version of the manuscript.

**Funding:** This research was supported by the Science and Technology Project of Hubei Province (2022EHB020), the National Natural Science Foundation of China (U21B2073), and the Science and Technology Innovation Plan of Hunan Province (2022RC3033, 2021GK2009). We also greatly appreciate the support from the Powder Metallurgy Institute of Central South University and CRRC Industrial Research Institute.

**Data Availability Statement:** All data included in this paper are available upon request by contact with the corresponding authors.

**Conflicts of Interest:** The authors declare no conflict of interest.

## References


1. Zhe, J.; Zhu, H.; Qiu, Y. Microstructure and Mechanical Properties of 7B05 Aluminum Alloy repaired by Laser Additive with Al, Mg, Sc, Zr Aluminum Alloy Powder. *Mod. Urban Rail Transit* **2022**, *5*, 87–93.
2. Lv, F.; Shen, L.; Liang, H. Mechanical properties of AlSi10Mg alloy fabricated by laser melting deposition and improvements via heat treatment. *Optik* **2019**, *179*, 8–18. [CrossRef]
3. Svetlizky, D.; Zheng, B.; Buta, T. Directed energy deposition of Al 5xxx alloy using Laser Engineered Net Shaping (LENS (R)]. *Mater. Des.* **2020**, *192*, 108763. [CrossRef]
4. Deng, S.; Zhao, H.; Li, R. Composition design of low hot-cracking susceptibility of Al-Zn-Mg-Sc alloy and its formability during laser additive manufacturing. *Mater. Charact.* **2022**, *193*, 112304. [CrossRef]
5. Anika, L.; Bohlen, A.; Rentsch, R. Mechanical Properties of High Strength Aluminum Alloy EN AW-7075 Additively Manufactured by Directed Energy Deposition. *Metals* **2020**, *10*, 579.
6. Benoit, M.J.; Sun, S.D.; Brandt, M. Processing window for laser metal deposition of Al 7075 powder with minimized defects. *J. Manuf. Process.* **2021**, *64*, 1484–1492. [CrossRef]
7. Wang, X.; Chen, J.; Lin, X. Repair of 7050 aluminum Alloy by AlSi12 powder laser Forming. *Chin. J. Lasers* **2009**, *36*, 1585–1590. (In Chinese) [CrossRef]
8. Hou, Y.; Liu, C.; Dai, H. Effects of Scandium Addition and Heat Treatment on Microstructure and Mechanical Properties of 7 Series Aluminum Alloy in Friction Stir Processing. *J. Heat Treat. Mater.* **2020**, *41*, 32–38. (In Chinese)
9. Pan, W.; Zhai, Z.; Liu, Y. Research on Microstructure and Cracking Behavior of Al-6.2Zn-2Mg-xSc-xZr Alloy Fabricated by Selective Laser Melting. *Crystals* **2022**, *12*, 1500. [CrossRef]
10. Bi, J.; Lei, Z.; Chen, Y. Microstructure and mechanical properties of a novel Sc and Zr modified 7075 aluminum alloy prepared by selective laser melting. *Mater. Sci. Eng.* **2019**, *768*, 138478. [CrossRef]
11. Liu, J.; Chen, H.; Wei, J. Micro-zone Softening Behavior and Control of Friction Stir Welded Joint of 7N01-T5 Aluminum Alloy. *Light Alloy Process. Technol.* **2021**, *49*, 58–67. (In Chinese)
12. Li, N.; Wang, Y.; Zhou, Z. Microstructure and Mechanical Properties of 7075 Aluminum Alloy Friction Stir Processing Zone. *Hot Work. Technol.* **2019**, *48*, 95–100. (In Chinese)
13. Zhu, H.; Hua, Q.; Li, R. Microstructure and Mechanical properties of 5083 Aluminum alloy repaired by laser directed Energy Deposition Additive. *Powder Metall. Mater. Sci. Eng.* **2022**, *27*, 45–55. (In Chinese)
14. Zhang, Y. *Research on Laser Adding and Reducing Material Repairing Aluminum Alloy Casing*; Shenyang Aeronautics and Astronautics University: Shenyang, China, 2019. (In Chinese)
15. Bhagavatam, A.; Ramakrishnan, A.; Adapa, V.S.K. Laser metal deposition of aluminum 7075 alloy. *Int. J. Mater. Sci. Res.* **2017**, *719*, 151–158. [CrossRef]
16. Tang, H.; Li, R.; Zhu, H. Microstructure and Mechanical properties of Al-Zn-Mg-Cu aluminum Alloy substrate repaired by laser directed deposition of Al-Mg-Sc Alloy powder. *Powder Metall. Mater. Sci. Eng.* **2022**, *27*, 111–120. (In Chinese)
17. Hu, Z. *Study on Microstructure and Properties of High Strength Aluminum Alloy Al7075 Additive Manufacturing*; Guizhou University: Guiyang, China, 2021. (In Chinese)
18. Bi, J.; Lei, Z.; Chen, X. Microstructure and mechanical properties of TiB2-reinforced 7075 aluminum matrix composites fabricated by laser melting deposition. *Ceram. Int.* **2019**, *45*, 5680–5692.
19. Xu, R.; Wang, W.; Zhu, H. Study on Microstructure and properties of 5083-H112 Aluminum Alloy repaired by laser Directed Energy Deposition Al-Mg-Sc-Zr. *J. Mater. Eng.* **2002**, *10*, 11868. (In Chinese)
20. Wang, Z.; Lin, X.; Tang, Y. Laser-based directed energy deposition of novel Sc/Zr-modified Al-Mg alloys: Columnar-to-equiaxed transition and aging hardening behavior. *J. Mater. Sci. Technol.* **2021**, *69*, 168–179. [CrossRef]
21. Liu, J.; Wang, X.; Zhang, Z. Study on Mechanical Properties of Welded Joints of Al-Mg-Zn Aluminum Alloy. *Electr. Weld. Mach.* **2017**, *47*, 142–145. (In Chinese)
22. Maria, L.; Montero, S.; Raya, M. Changing the alloy composition of Al7075 for better processability by selective laser meltin. *J. Mater. Process. Technol.* **2016**, *238*, 437–445.
23. Su, Y.; Wang, Y.; Shi, J. Microstructure and mechanical properties of laser DED produced crack-free Al 7075 alloy: Effect of process parameters and heat treatment. *Mater. Sci. Eng. A* **2022**, *857*, 144075. [CrossRef]
24. Chen, K.; Zheng, X.; Zhang, Y. Study on Heat Treatment Process of New 7XXX Series Aluminum Alloy. In Proceedings of the 2019 Academic Annual Meeting of the Chinese Nuclear Society, Baotou, China, 20 August 2019. (In Chinese).


**Disclaimer/Publisher's Note:** The statements, opinions and data contained in all publications are solely those of the individual author(s) and contributor(s) and not of MDPI and/or the editor(s). MDPI and/or the editor(s) disclaim responsibility for any injury to people or property resulting from any ideas, methods, instructions or products referred to in the content.